

# Monitoring of Actuation Conditions in a Micro-Turbo-Generator

Mustafa Ilker Beyaz, *Member, IEEE*, Brendan Hanrahan, Jeremy Feldman, and Reza Ghodssi, *Member, IEEE*

**Abstract**—This paper presents the theory and implementation of an integrated sensing technique for the real-time measurement of applied actuation conditions in a micro-turbo-generator. The device is composed of a microturbine rotor with magnetic components and a stator with planar coils for electromagnetic induction. While the rotor is actuated with pressurized nitrogen, the induced voltages are extracted to generate and deliver electrical power as well as to monitor the pneumatic actuation parameters. It is demonstrated that the rotor speed, applied gas flow rate, and pressure show repeatable high linearity with respect to voltage frequency and amplitude in different devices. Sensitivity values of 83 Hz/krpm, 140 Hz/slm, and 1428 Hz/psi together with  $R^2$  values larger than 0.97 are achieved. The integrated sensing technique presented in this paper will eliminate the need for external sensing components in continuous device screening, and lead to closed-loop control for autonomous tuning of desired operating conditions in rotary microgenerators.

**Index Terms**—Micro generator, turbogenerator, actuation conditions, integrated sensing, power MEMS.

## I. INTRODUCTION

**P**OWER conversion at the small scale is a fast-advancing field due to the growing power demands of portable electronic systems. Rotational electromagnetic microgenerators could meet these power demands with potential generation capability from microwatts to watts. Accordingly, significant research efforts have been dedicated to develop rotary microgenerators with various electromagnetic and mechanical architectures [1]–[11].

Rotational microgenerators generally consist of a rotor and a stator, and convert mechanical/pneumatic actuation into usable electricity. The previous demonstrations of these devices have been actuated using (i) external spindles or (ii) pressurized gas flow. In both cases, these devices were shown to operate under a wide range of rotational speeds, which has a quadratic

impact on generated power [1]–[11]. Pan presented a micro-generator that was actuated with an external mechanical drive mechanism, capable of reaching 13krpm, ultimately resulting in milli-watt range output power [1], [2]. A three-phase axial flux permanent magnet generator with a low-impedance stator was demonstrated by Arnold *et al.* [3], [4]. Using a similar actuation technique, DC powers up to 8 W were achieved at rotor speeds as high as 305 krpm. Herrault presented the further miniaturization of this device down to a rotor diameter of 2 mm [5]. The rotor was reported to approach 400 krpm and provide 6.6 mW output power on a matched electrical load. Same authors later improved the performance of the device in [4] using a laminated stator, and reported watt-level power generation at 200 krpm [6].

In addition to speed, applied actuation conditions further extend to include gas flow rate and pressure for pneumatically actuated integrated micro-turbo-generators. Holmes developed a micro-turbo-generator to extract power from an externally generated gas stream. At the reported values of 35 slm and 8mbar pressure drop, the turbine rotor reached 30 krpm [7]. Raisigel demonstrated a microgenerator with turbine structures defined on the permanent magnet rotor that is supported on magneto-pneumatic bearings [8]. The rotor was spun with 5 bar gas supply up to a speed of 100 krpm. Higher speeds on the order of 400 krpm were also reported using a dental drill. The first micro-turbo-generator supported on gas bearings was presented by Yen for power generation at supercritical speeds [9]. The rotor of the device reached 40 krpm at journal bearing pressure differences on the order of 0.2 psi. More recently, our team has reported the development of a micro-turbo-generator supported on encapsulated microball bearings, and demonstrated successful device operation up to a rotor speed of 23 krpm that required a gas flow rate of 12.6 slm and a pressure of 1.2 psi across the device [10], [11].

The wide-ranging actuation conditions, i.e. speed, flow rate, and pressure values, resulted in various levels of device performance and output power in different prototype micro-generators. Although the current efforts are dedicated to developing high-power devices, it is equally significant and critical to develop integrated sensing techniques to monitor the operational conditions for several important reasons: (i) The eventual integration of microgenerators with other microsystems requires an integrated mechanism to actively measure and control the actuation without external testing components or off-the-shelf sensors. (ii) Precise determination of the real time actuation state is vital for remaining in the safe operation and stability range as well as for the reliability of microgenerators. (iii) Autonomous tuning of the desired mechanical and

Manuscript received January 31, 2013; revised March 22, 2013 and April 13, 2013; accepted April 13, 2013. Date of publication April 23, 2013; date of current version July 2, 2013. This work was supported by the U.S. National Science Foundation under Award 0901411. The associate editor coordinating the review of this paper and approving it for publication was Prof. Weileun Fang.

M. I. Beyaz was with the University of Maryland, College Park, MD 20742 USA. He is now with the Department of Electrical and Electronics Engineering, Antalya International University, Antalya 07190, Turkey (e-mail: mibeyaz@antalya.edu.tr).

B. Hanrahan is with the University of Maryland, College Park, MD 20742 USA, and also with the U.S. Army Research Laboratory, Adelphi, MD 20783 USA (e-mail: bhanrah@gmail.com).

J. Feldman and R. Ghodssi are with the University of Maryland, College Park, MD 20742 USA (e-mail: jfn@umd.edu; ghodssi@umd.edu).

Color versions of one or more of the figures in this paper are available online at <http://ieeexplore.ieee.org>.

Digital Object Identifier 10.1109/JSEN.2013.2259477

electrical parameters necessitates closed-loop control, which in turn requires integrated monitoring of the applied actuation. Accordingly, this work is focused on developing a technique for the real-time sensing of actuation conditions in microgenerators without external sensors. The method presented here uses the already-induced voltages for power generation, and hence, provides an integrated sensing mechanism to determine the actuation speed, applied gas flow rate, and pressure. Initial results of this work have been recently presented in [12]. In this paper, we describe the theoretical background behind device monitoring, and extend our results to demonstrate repeatability among different devices.

## II. DESIGN AND THEORY

The microgenerator described here is a turbo generator actuated by pressurized nitrogen flow, and is comprised of a rotor supported on microball bearings suspended above a stator. The rotor is composed of two 500  $\mu\text{m}$ -thick silicon wafers bonded together, and measures 6 mm in radius. Microballs ( $\text{O} = 285 \mu\text{m}$ ) are placed in between the bonded wafers within pre-etched trenches (Figure 1). The top side of the rotor has 200  $\mu\text{m}$ -tall turbine structures for pneumatic actuation, while the bottom side of the rotor is allocated for accommodating ten NdFeB permanent magnets and a high-permeability FeCoV disc. The magnets are arranged in alternating polarity to create a time varying magnetic flux synchronized with rotor rotation (Figure 1b). To direct the gas flow and actuate the rotor, a silicon plumbing chip with one central and several peripheral through holes is placed on top of the rotor (Figure 1a). The stator is composed of three-phase, ten-pole, and several turns-per-pole Cu coils embedded in a 400  $\mu\text{m}$ -thick thermally oxidized silicon substrate (Figure 2). The radial parts of the coils are serially connected through the inner and outer Cu lines over a dielectric layer on the backside of the stator.

The device is packaged in an upside-down orientation using acrylic components and compliant O-rings (Figure 1d). During operation, the nitrogen flow enters the system through the peripheral holes on the plumbing chip, spins the rotor, and leaves the device from the center (packaging components are not shown). Since the gas can leak to the sealed backside of the rotor through the microball bearings, the flow path of the nitrogen results in a pressure build up, and hence a net upward force on the bearings. In such operation, the rotor speed, gas flow rate, and pressure drop across the device should be constantly monitored for the previously explained reasons.

The rotation of the rotor together with the permanent magnets induces AC voltages across the terminals of the coils due to Faraday's law of electromagnetic induction, which can be simplified to the following form [10], [11]:

$$V = A \times \frac{dB_{avg}(t)}{dt}. \quad (1)$$

Here,  $A$  is the area of one coil loop and  $B_{avg}(t)$  is the average magnetic flux density varying in a triangular waveform between  $\pm B_{avg}$ . In such a device with  $P$  number of magnetic poles on the rotor spinning at  $\omega$  rpm (rotations per minute), the electrical frequency of the induced voltage becomes:

$$f = \frac{P}{2} \times \frac{\omega}{60}. \quad (2)$$

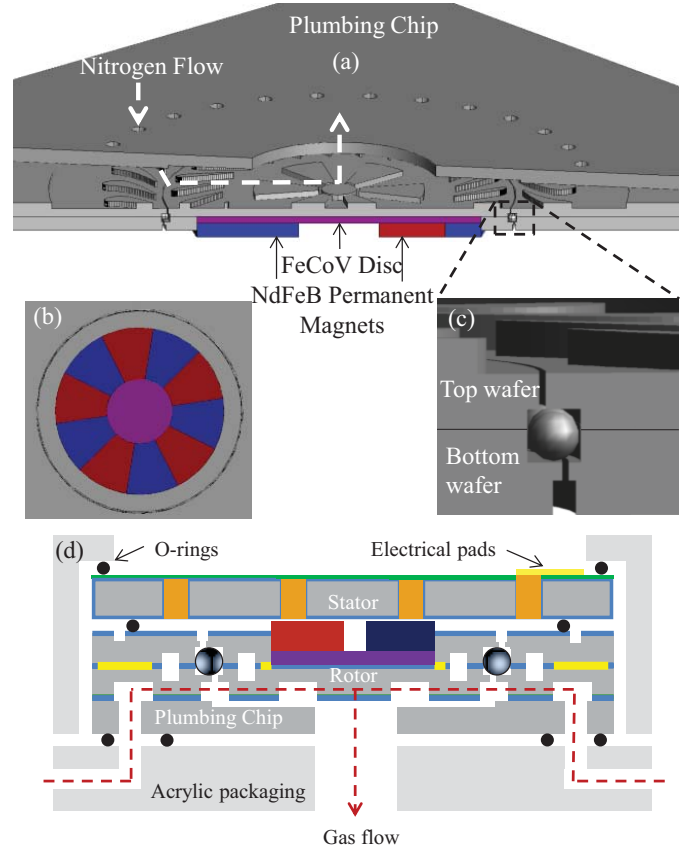


Fig. 1. 3D schematic views of the rotor showing (a) general structure and actuation, (b) permanent magnets on the bottom, and (c) encapsulated microball bearings, (d) upside-down testing scheme [10].

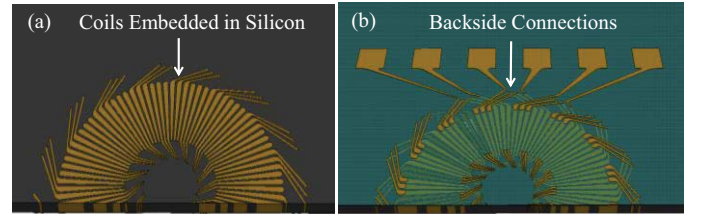


Fig. 2. 3D cutaway schematics of the stator showing (a) Cu coils embedded in silicon and (b) backside connections over a dielectric layer [10].

Combining equations (1) and (2), and replacing the area as  $A = (\pi \times (r_{out}^2 - r_{in}^2))/P$ , with  $r_{out}$  and  $r_{in}$  being the outer and inner radii of the radial parts, for an  $N$ -turns-per-pole stator we obtain [10], [11]:

$$V = \frac{P \times N \times B_{avg} \times \pi \times (r_{out}^2 - r_{in}^2) \times \omega}{60}. \quad (3)$$

As seen from equations (2) and (3), the induced voltage amplitude  $V$  and frequency  $f$  are directly proportional to speed, where proportionality coefficients are time-invariant device parameters. This shows that the speed resulting from pneumatic actuation can be determined by measuring either the voltage amplitude or frequency.

Although it is not possible to derive immediate expressions for the flow rate and pressure in terms of the voltage in micro-turbines, researchers have developed experimental approaches

to reveal the relationship between flow rate, pressure and speed, which can then be related to voltage through equations (2) and (3). McCarthy reported the performance and experimental analysis of an integrated microball bearings-supported microturbine in [13]. It was empirically demonstrated that the pressure versus speed and flow rate data show virtually linear behavior up to the maximum characterization speed of 10 krpm [13]. Considering the speed is directly proportional to the voltage frequency and amplitude as dictated by equations (2) and (3), these results suggest that the applied flow rate and pressure should also linearly change with respect to voltage frequency and amplitude in a micro-turbo-generator supported on microball bearings.

### III. FABRICATION

The details of the microfabrication process were explained in [10], [11], and briefly summarized here. Figure 3 provides a cross-sectional schematic of the fabrication sequence. Initially, ball raceways are patterned on two rotor wafers using the deep reactive ion etching (DRIE) technique (Figure 3a). Next, the microballs are placed in the raceway with an 80% fill factor. Eutectic AuSn alloy is evaporated on the surface of the wafer, and then the two wafers are bonded together by melting and re-solidifying the alloy under pressure (Figure 3b). Subsequent DRIE steps are performed on top and bottom sides of the bonded wafers to release the rotor from the stationary frame, to define turbine structures on the top side, and to create a space for housing magnetic components on the bottom side (Figure 3c). A FeCoV disc and ten NdFeB magnets are assembled and incorporated to the rotor housing using epoxy. In parallel, the silicon plumbing chip is fabricated through sequential DRIE steps on top and bottom sides to define one central and several peripheral through holes. A short cavity is also created on the bottom side that would ensure a safety margin between rotor turbine blades and the plumbing chip during actuation (Figure 3d).

The stator wafer is fabricated through a series of DRIE, material deposition, and patterning processes. First, the coil housings are defined using DRIE, and the stator wafer is thermally oxidized for electrical isolation (Figure 3e). Subsequently, a bottom-up electroplating technique presented in [14] is applied for conformal filling of the housings with copper (Figure 3f). A KMPR 1050 layer is spun and patterned on the stator backside to define vias and provide further isolation for the next metal layer. Next, gold is sputtered and patterned over KMPR 1050 to complete the coil connections (Figure 3g). Finally, the device is assembled leaving a 200 – 700  $\mu\text{m}$  air gap between the rotor and the stator (Figure 3h). Two devices are fabricated: (i) 10-pole rotor and 10-pole 2-turns-per-pole stator, and (ii) 10-pole rotor and 3-turns-per-pole stator. The photographs of a fabricated device are shown in Figure 4.

### IV. TESTING AND DISCUSSIONS

Figure 5 shows a photograph of a micro-turbo-generator packaged with acrylic components and O-rings for actuation. To perform testing and characterization, pressurized nitrogen

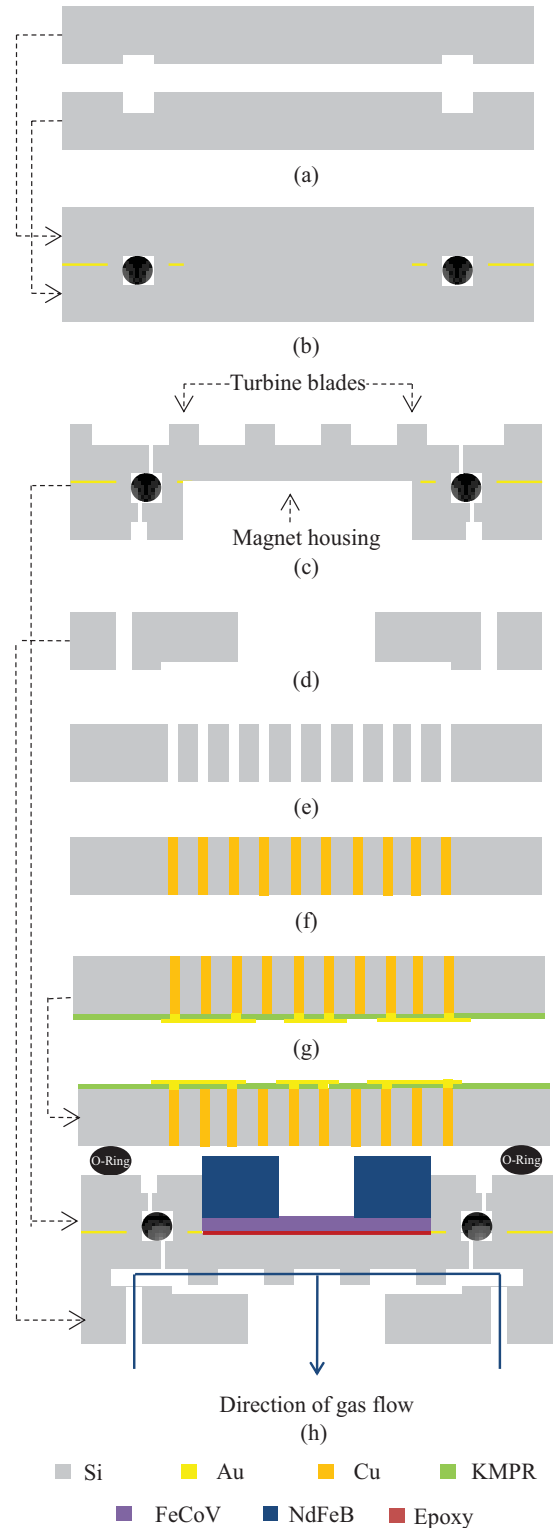


Fig. 3. Fabrication flow of the (a–d) rotor with turbine blade structures, magnetic housing, and a separate chip for gas flow, (e–g) stator with through-plated copper integrated in silicon and a second level of metallization, and (h) assembled device [10], [11].

was applied to the device through fluidic ports in the packaging. While the nitrogen flow rate was measured by an external flow sensor serially connected between the gas supply and the corresponding fluidic ports, gas pressure across the device was monitored by a pressure sensor connected to a different

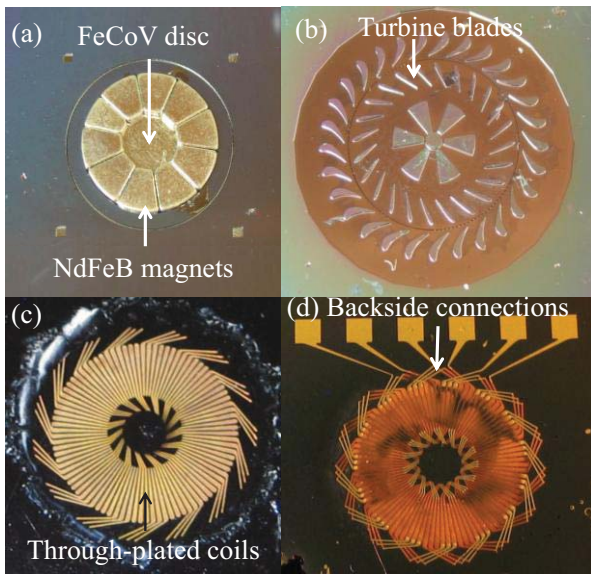


Fig. 4. Pictures of a fabricated device. (a) Rotor bottom view. (b) Rotor top view. (c) Stator top view. (d) Stator bottom view [10], [11].

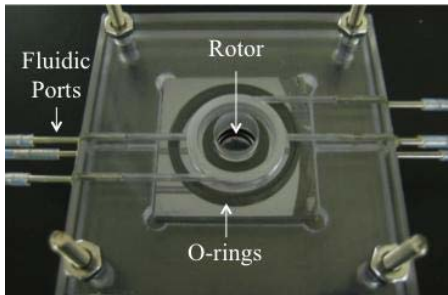


Fig. 5. Picture of a packaged device.

set of fluidic ports on the package. This connection scheme is specifically useful to exclude the pressure drops along the tubing/fluidic ports, and to precisely measure actuation pressure. An optical displacement sensor was employed in the test setup to detect pre-etched structures on the rotor for speed measurements. To measure and analyze the speed, flow rate, and pressure as well as to record the induced voltages on the stator, a Labview program utilizing Fast Fourier Transform (FFT) algorithms were implemented with a voltage sampling resolution on the order of 1 mV. The 10-pole 2-turns-per-pole device (D1) was tested at rotational speeds up to 16 krpm, while the 10-pole 3-turns-per-pole device (D2) was tested up to 23 krpm, above which the operation could not be performed due to imperfections in the fabrication and packaging. Voltage induction and power generation performances were presented in [10], [11].

#### A. Rotor Speed

The variations of rotor speed with respect to voltage frequency and amplitude are plotted for the two fabricated devices on Figure 6. The linear curve fits show that the data exhibit linear behavior up to the tested speeds with  $R^2$  values larger than 0.99. As seen on Figure 6a, the speed versus frequency curves for the two devices lie on top of each other.

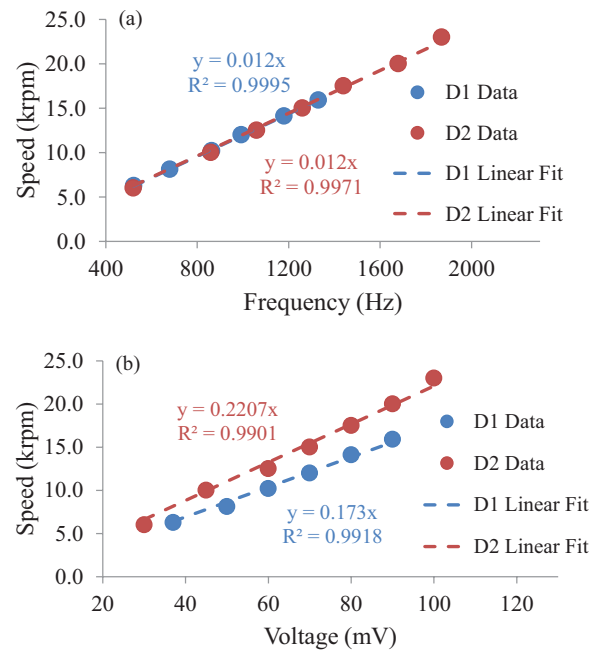


Fig. 6. Rotor speed versus (a) voltage frequency and (b) voltage amplitude.

This is consistent with equation (2), where frequency is related to speed only with the number of poles that are equal for the two devices. In addition, the frequency sensitivity is calculated to be 83 Hz/krpm, which is the exact value resulting from equation (2), demonstrating the perfect agreement between the theory and experimental data. Although linear, the dependency of speed to voltage amplitude is different for D1 and D2. This is due to the difference in turns-per-pole parameters and air gaps, and slight changes in the magnetic flux density within the two devices, which lead to different voltage levels as indicated by equation (3). The resulting voltage sensitivity values are calculated to be 5.7 mV/krpm for D1 and 4.5 mV/krpm for D2. Data below 5 krpm is not presented due to the static friction in the bearings setting a threshold for actuation.

#### B. Flow Rate and Pressure

Figure 7 shows the measured flow rate values with respect to voltage frequency and amplitude for both devices. The data again show linear behavior with  $R^2$  values between 0.97 and 0.99, supporting the above discussions and previous findings reported in [13]. The resulting sensitivity values are calculated to be 71 Hz/slm and 4.5 mV/slm for D1, and 140 Hz/slm and 7.5 mV/slm for D2. Similar to speed versus voltage amplitude data, there is no overlap between device datasets as seen in Figure 7. This is attributed to the slight variations in the fabrication and packaging of the two devices, which considerably affect the fluidic performance. These variations may be the disparities in turbine blade height, ball raceway profile, number of microballs in the raceway, rotor-stator air gap, number of turns per pole, and gas leakages in the package. As a result, the graphs on Figure 7a and 7b have different slopes for the two devices, showing that different amounts of flow rates are required to actuate the rotors at a given desired speed.

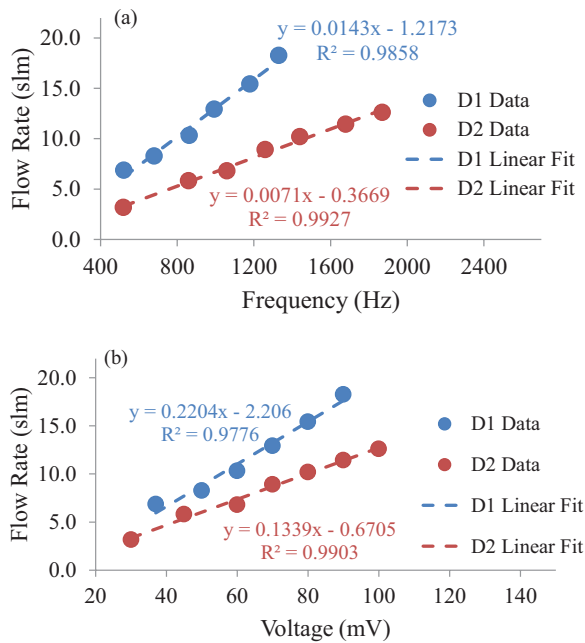


Fig. 7. Flow rate versus (a) voltage frequency and (b) voltage amplitude.

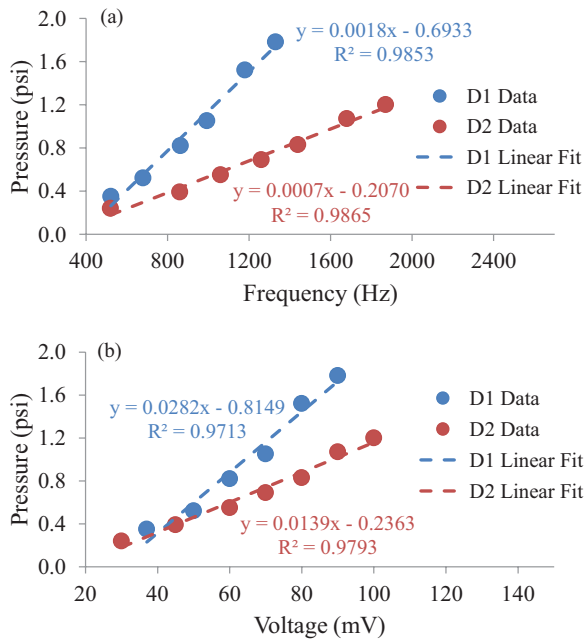


Fig. 8. Pressure versus (a) voltage frequency and (b) voltage amplitude.

The same effect is also observed in the pressure versus voltage characteristics on Figure 8. Although very close, the curve slopes are different for D1 and D2. The linear curve fits show  $R^2$  values higher than 0.97 for all four data sets. From the slopes of these curves, the sensitivity values are calculated to be 1000 Hz/psi and 35 mV/psi for D1, and 1428 Hz/psi and 72 mV/psi for D2.

The repeatable linearity of the data in different devices along with the sensitivity values reported above demonstrate that the already-generated voltages can be used for real-time sensing of the rotor speed, flow rate, and pressure. The inevitable

dissimilarities in the devices after fabrication and packaging, however, mandate a characterization process to determine the actual curve slope, sensitivity, and the lowest speed threshold specific to each device. Accordingly, an initial test operation is necessary to obtain the voltage-actuation relationship as well as to determine the minimum speed, flow rate, and pressure above which each device can be reliably actuated. Once these correlations and parameters are revealed, the generated voltages can be reliably utilized to monitor the real-time actuation conditions for the following operations. It should be noted that two important aspects, namely high-speed regime and prolonged operations, are not addressed in this paper due to fabrication and testing complexities explained in [11]. The observed linearity between the voltage and actuation up to 23 krpm can not be directly extrapolated for elevated speeds. Although rotational speeds in close proximity may exhibit the same linearity, several nonlinear factors such as wear and fluidic losses may come into play at higher speeds and lead to deviations from the linear behavior. In addition, device tests aimed at several days to weeks of operation can shed light on the long-term performance of the sensing mechanism reported here. These two aspects will be investigated in future studies by manufacturing and characterizing more devices using an improved fabrication process and testing scheme.

There are several ways to improve the sensitivity of the measurements. First, the number of magnetic poles on the rotor can be increased to achieve a higher change in frequency per unit speed as indicated in equation (2). However, deviating from the optimum number of poles comes at the expense of lower magnetic flux linkage to the stator due to higher number of magnetic transition regions between adjacent permanent magnets. As a direct result, the magnetic leakage will increase and output power of the micro-turbo-generator will decrease. Alternatively, the air gap between the rotor and the stator can be lowered down to 50  $\mu\text{m}$  by including additional steps in the fabrication to yield a larger magnetic flux density within the stator. This will, as shown by equation (3), enhance the voltage amplitude per unit speed, flow rate, and pressure. Finally, the  $P \times N$  product in the same equation can be maximized to improve the sensitivity. This product defines the number of radial coil lines on the stator, and should be carefully selected to remain within the process limitations defined by the stator fabrication techniques.

The integrated sensing technique presented here provides an opportunity to implement a closed-loop control system for autonomous and active tuning of the desired performance as well as a stable operation. This can be achieved by designing a circuitry that can (i) read the induced voltage amplitude and frequency, (ii) make a comparison between the current and desired actuation states, and (iii) generate the necessary error signal to regulate the actuation. Depending on the required overall device performance, this error signal can be fed into a proportional (P) or a more sophisticated PID (proportional-integral-derivative) controller designed for the specific system needs. As a result, precise control on the output voltages as well as applied fluidic flow rate, pressure, and rotational speed can be achieved autonomously and adaptively, which will enhance device reliability, stability, and lifetime.

## V. CONCLUSION

The theory and implementation of an integrated sensing technique to monitor the actuation conditions of a micro-turbo-generator is presented. Composed of a turbine rotor with magnetic components and a stator with planar coils, the device generates voltage and power in response to pneumatic actuation. It has been demonstrated that the induced voltage frequency and amplitude show repeatable linearity with respect to actuation parameters among different devices in accordance with the theoretical analysis up to the maximum tested speed of 23 krpm.  $R^2$  values larger than 0.97 together with sensitivity values as high as 83 Hz/krpm, 140 Hz/slm, and 1428 Hz/psi were obtained for the speed, flow rate, and pressure, respectively. Strategies to improve the sensitivity as well as to implement a closed-loop control system were discussed. Future work will focus on high-speed and long-term characterization of the sensing technique reported here. The linearity between the electrical signals and actuation parameters shows that the generated voltages can provide an integrated sensing mechanism, which could ultimately replace external off-the-shelf sensors in real-time device monitoring. The technique described here will lead to closed-loop control in rotary microgenerators for autonomous and active tuning of the desired performance as well as enhanced reliability, stability, error compensation, and lifetime.

## REFERENCES

- [1] C. T. Pan and Y. J. Chen, "Application of low temperature co-fire ceramics on in-plane micro-generator," *Sens. Actuators A, Phys.*, vol. 144, pp. 144–153, May 2008.
- [2] C. T. Pan and T. T. Wu, "Development of a rotary electromagnetic microgenerator," *J. Micromech. Microeng.*, vol. 17, no. 1, pp. 120–128, Jan. 2007.
- [3] D. P. Arnold, S. Das, J.-W. Park, I. Zana, J. H. Lang, and M. G. Allen, "Microfabricated high-speed axial-flux multiwatt permanent-magnet generators—Part II: Design, fabrication, and testing," *J. Microelectromech. Syst.*, vol. 15, pp. 1351–1363, Oct. 2006.
- [4] D. P. Arnold, F. Herrault, I. Zana, P. Galle, J.-W. Park, S. Das, J. H. Lang, and M. G. Allen, "Design optimization of an 8 W, microscale, axial-flux, permanentmagnet generator," *J. Micromech. Microeng.*, vol. 16, pp. S290–S296, Sep. 2006.
- [5] F. Herrault, C.-H. Ji, and M. G. Allen, "Ultraminaturized, high-speed, permanent magnet generators for milliwatt-level power generation," *J. Microelectromech. Syst.*, vol. 17, no. 6, pp. 1376–1387, Dec. 2008.
- [6] F. Herrault, B. C. Yen, C. H. Ji, Z. S. Spakovszky, J. H. Lang, and M. G. Allen, "Fabrication and performance of silicon-embedded permanent-magnet microgenerators," *J. Microelectromech. Syst.*, vol. 19, no. 1, pp. 4–13, Feb. 2010.
- [7] A. S. Holmes, G. Hong, and K. R. Pullen, "Axial-flux permanent magnet machines for micropower generation," *J. Microelectromech. Syst.*, vol. 14, no. 1, pp. 54–62, Feb. 2005.
- [8] H. Raisigel, O. Cugat, and J. Delamare, "Permanent magnet planar microgenerators," *Sens. Actuators A, Phys.*, vol. 130, pp. 438–444, Aug. 2006.
- [9] B. C. Yen, F. Herrault, K. J. Hillman, M. G. Allen, F. F. Ehrich, S. Jacobson, C.-H. Ji, J. H. Lang, H. Li, Z. S. Spakovszky, and D. R. Veazie, "Characterization of a fully-integrated permanent-magnet turbine generator," in *Proc. Power MEMS*, Nov. 2008, pp. 121–124.
- [10] M. I. Beyaz, B. Hanrahan, J. Feldman, and R. Ghodssi, "An integrated electromagnetic micro-turbo-generator supported on encapsulated microball bearings," in *Proc. IEEE 25th Int. Conf. Micro Electro Mech. Syst.*, Jan. 2012, pp. 1209–1212.
- [11] M. I. Beyaz, B. Hanrahan, J. Feldman, and R. Ghodssi, "An integrated permanent magnet micro-turbo-generator supported on microball bearings," *J. Microelectromech. Syst.*, Jan. 2013, to be published.
- [12] M. I. Beyaz, B. Hanrahan, J. Feldman, and R. Ghodssi, "Integrated sensing of mechanical parameters in a micro-turbo-generator," in *Proc. IEEE Sensors*, Oct. 2012, pp. 1–4.
- [13] M. McCarthy, C. M. Waits, and R. Ghodssi, "Dynamic friction and wear in a planar-contact encapsulated microball bearing using an integrated microturbine," *J. Microelectromech. Syst.*, vol. 18, no. 2, pp. 263–273, Apr. 2009.
- [14] M. I. Beyaz, M. McCarthy, and R. Ghodssi, "Fabrication of high-aspect ratio metal structures with planar surfaces for power MEMS devices," in *Proc. Power MEMS*, Dec. 2009, pp. 586–588.



**Mustafa Ilker Beyaz** received the B.S. degree in electrical and electronics engineering from Middle East Technical University, Ankara, Turkey, in 2005, and the M.S. and Ph.D. degrees in electrical engineering from the University of Maryland (UMD), College Park, MD, USA, in 2008 and 2011, respectively.

He joined the Department of Electrical and Electronics Engineering, Antalya International University, Antalya, Turkey, as an Assistant Professor in 2011, where he leads research activities in MEMS.

His current research interests include primarily in the design and development of microsystems for power conversion and energy harvesting, development of biological sensors and actuators, and the application of nanostructured materials to MEMS devices.

Dr. Beyaz is a member of the IEEE Society and served on the technical program committee of the IEEE Sensors 2012 conference. He is also serving as a peer reviewer for major MEMS journals. He was the recipient of two doctoral research awards from the Department of Electrical and Computer Engineering and James Clark School of Engineering, UMD.



**Brendan Michael Hanrahan** received the B.S. degree in ceramic and materials engineering from Clemson University, Clemson, SC, USA, in 2006, and the M.S. and Ph.D. degrees in materials science and engineering from the University of Maryland, College Park, MD, USA, in 2009 and 2013, respectively.

He has been a Materials Engineer with the U.S. Army Research Lab in the Sensors and Electron Devices Directorate, since 2009. His current research interests include the tribology of high performance microelectromechanical systems (MEMS) and the development of MEMS components for compact, portable power systems.



**Jeremy Feldman** received the Bachelor of Science degree in electrical engineering from the University of Maryland, College Park, MD, USA, in 2011, with concentrations in microelectronics, nanomaterials, and power systems, where he is currently pursuing the Masters degree in systems engineering with a focus in optical methods for bio-sensing, and bio-feedback systems.

His undergraduate research was in high density thin film capacitors, optical structured nanomaterials for photovoltaics and sensors, nano level security markers, as well as an extensive study of vibration and wear in rotary MEMS devices supported on microball bearing technology. He is currently conducting research at the MEMS Sensors and Actuators Laboratory, University of Maryland.



**Reza Ghodssi** (S'92–M'96) received the B.Sc., M.Sc., and Ph.D. degrees from the Electrical Engineering Department, University of Wisconsin, Madison, WI, USA, in 1990, 1992, and 1996, respectively.

He is currently the Herbert Rabin Distinguished Chair in Engineering, the Director of the Institute for Systems Research, and the Director of the MEMS Sensors and Actuators Laboratory, Department of Electrical and Computer Engineering, University of Maryland (UMD), College Park, MD, USA. He is also currently with the Fischell Department of Bioengineering, Maryland NanoCenter, University of Maryland Energy Research Center, and the Materials Science and Engineering Department, UMD. He has over 95 referred journal publications. He was the Co-editor of the Handbook of *MEMS Materials and Processes* (published in 2011). His research interests are in the design and development of microfabrication technologies and their applications to micro/nanodevices and systems for chemical and biological sensing, small-scale energy conversion, and harvesting.

Dr. Ghodssi is a member of the American Vacuum Society, the Materials Research Society, the American Society for Engineering Education, and the American Association for the Advancement of Science. He is an Associate Editor for the *Journal of Microelectromechanical Systems and Biomedical Microdevices*. He was the Chair of the NSF Workshop on Micro Nano Bio Systems in 2012. He was also the Chair of the Ninth International Workshop on Micro and Nanotechnology for Power Generation and Energy Conversion Applications, also known as “PowerMEMS 2009” and the Americas Technical Program Committee Chair of the IEEE Sensors 2010, 2011, and 2012 Conferences. He is the Co-Founder of MEMS Alliance in the greater Washington area. He was the recipient of the 2001 UMD George Corcoran Award, the 2002 National Science Foundation CAREER Award, and the 2003 UMD Outstanding Systems Engineering Faculty Award.